HHS Public Access

Author manuscript

Adv Funct Mater. Author manuscript; available in PMC 2018 January 05.

Published in final edited form as:

Adv Funct Mater. 2017 January 5; 27(1): . doi:10.1002/adfm.201604872.

A Cooperative Copper Metal-Organic Framework-Hydrogel System Improves Wound Healing in Diabetes

Dr. Jisheng Xiao[1], **Siyu Chen**[1], **Dr. Ji Yi**[1], **Dr. Hao Zhang**[1,3], and **Dr. Guillermo A. Ameer**[1,2,3,4,*]

[1]Biomedical Engineering Department, Northwestern University, 2145 Sheridan Road, Evanston, IL 60208, USA

[2]Department of Surgery, Feinberg School of Medicine, Chicago, Illinois 60611, United States

[3]Chemistry of Life Processes Institute, Northwestern University, Evanston, IL, 60208

[4]Simpson Querrey Institute, Northwestern University, Chicago, IL, 60611

Abstract

Chronic non-healing wounds remain a major clinical challenge that would benefit from the development of advanced, regenerative dressings that promote wound closure within a clinically relevant time frame. The use of copper ions has shown promise in wound healing applications possibly by promoting angiogenesis. However, reported treatments that use copper ions require multiple applications of copper salts or oxides to the wound bed, exposing the patient to potentially toxic levels of copper ions and resulting in variable outcomes. Herein we set out to assess whether copper metal organic framework nanoparticles (HKUST-1 NPs) embedded within an antioxidant thermoresponsive citrate-based hydrogel would decrease copper ion toxicity and accelerate wound healing in diabetic mice. HKUST-1 and poly-(polyethyleneglycol citrate-co-*N*-isopropylacrylamide) (PPCN) were synthesized and characterized. HKUST-1 NP stability in a protein solution with and without embedding them in PPCN hydrogel was determined. Copper ion release, cytotoxicity, apoptosis, and *in vitro* migration processes were measured. Wound closure rates and wound blood perfusion were assessed *in vivo* using the splinted excisional dermal wound diabetic mouse model. HKUST-1 NP disintegrated in protein solution while HKUST-1 NPs embedded in PPCN (H-HKUST-1) were protected from degradation and copper ions were slowly released. Cytotoxicity and apoptosis due to copper ion release were significantly reduced while dermal cell migration *in vitro* and wound closure rates *in vivo* were significantly enhanced. *In vivo*, H-HKUST-1 induced angiogenesis, collagen deposition, and re-epithelialization during wound healing in diabetic mice. These results suggest that a cooperatively stabilized, copper ion-releasing H-HKUST-1 hydrogel is a promising innovative dressing for the treatment of chronic wounds.

Graphical Abstract

*Corresponding Author: g-ameer@northwestern.edu.

Supporting Information

Supporting Information is available from the Wiley Online Library or from the author.

A copper ion-eluting thermoresponsive antioxidant hydrogel consisting of metal organic framework (HKUST-1) nanoparticles (NPs) and poly(polyethylene glycol citrate-co-*N*-isopropylacrylamide) (PPCN) was prepared and characterized (H-HKUST-1). H-HKUST-1 exhibited significantly reduced cytotoxicity and promoted the migration of dermal cells *in vitro. In vivo*, H-HKUST-1 promoted improved dermal wound closure rates in diabetic mice.

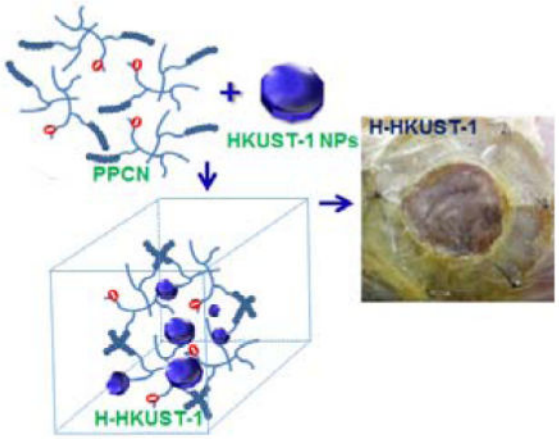

Keywords

copper metal-organic framework; hydrogel; wound healing; citric acid

1. Introduction

Chronic non-healing wounds continue to be a great challenge for physicians and contribute to increasing healthcare costs.[1] In particular, chronic diabetic foot ulcers (DFUs) are responsible for more than 73,000 nontraumatic lower limb amputations and impose a substantial cost burden on public and private payers, with costs ranging from $9–$13 billion in addition to the costs associated with diabetes itself.[2] Despite the use of autografts, tissue engineered products, and wound dressings of various types,[3] successful treatment of chronic DFUs remains elusive and currently there is no widely used effective therapy.[4] Therefore, new cost-effective, safe, and efficacious strategies are warranted to improve the care for hard-to-heal DFUs.

Non-pharmacological and non-biological strategies to address this problem are appealing because development time and regulatory costs are significantly lower if a product for medical therapy is classified as a medical device. In this regard, several approaches have been reported in the literature, including suction devices and the application of metal ions and small organic compounds.[1a, 5] Copper is an essential element with a long history of use in humans. It is involved in many wound-healing-related processes,[6] including induction of vascular endothelial growth factor,[5a] angiogenesis,[7] and the expression and stabilization of extracellular skin proteins, such as keratin and collagen.[8] Copper is also a well-known antimicrobial agent, which may contribute to improved healing by reducing the probability of infections in the wound. Copper sulfate and copper oxide were shown to promote healing

in healthy and diabetic BALB/c mice,[9] but multiple applications are necessary,[9c] putting the patient at risk of copper toxicity. Elevated non-physiological concentrations of copper ions can be toxic because the ions can interfere with the homeostasis of other metals, damage DNA, and generate reactive oxygen species that can adversely modify proteins, lipids and nucleic acids.[10] The median lethal dose (LD50) for mice exposed to copper ions via oral administration is 110 mg/kg body weight. The toxicity rating of copper ions is class 3 (moderately toxic) on the Hodge and Sterner Scale.[11] However, the toxicity may be alleviated if copper ions are slowly released from a depot placed at the desired location. Several studies on the slow release of copper ions have been reported; however, most of them focus on the reduction of a burst release of copper ions from intrauterine devices.[12] We hypothesize that slow release of copper ions can be achieved from copper benzene tricarboxylate $Cu_3(BTC)_2$, also known as HKUST-1 nanoparticles (NPs) when entrapped within an antioxidant citrate-based hydrogel and that the HKUST-1-hydrogel (H-HKUST-1) system will exhibit reduced cytotoxicity *in vitro* and enhance wound closure rates *in vivo* when used as a wound dressing.

Metal-organic frameworks (MOFs), also called porous coordination polymers, are a class of crystalline porous materials composed of inorganic metal ions or clusters connected by polydentate organic ligands.[13] They have been synthesized using a variety of organic ligands including ditopic, tritopic, tetratopic, hexatopic, octatopic, mixed, desymmetrized, metallo, and N-heterocyclic linkers.[14] MOFs have typically been used for gas adsorption and separation,[15] catalysis,[16] luminescence,[17] sensing,[18] proton conduction[19] and their properties could potentially be useful for biomedical applications.[20] Although potentially interesting for biomedical applications, MOFs tend to be not stable in physiological protein-containing solution.[21] However, Zhang et al. have shown that MOFs can be stabilized with surface coatings.[22] These findings open the possibility to use the entrapment of HKUST-1 NPs in hydrogels as a mechanism to slow down their degradation and thus prevent premature release of the cargo, [21] which potentially could render MOFs suitable for use in a wound bed.

As for the antioxidant hydrogel depot for sustained copper ion release, to our knowledge there are no published reports on the controlled release of copper ions from hydrogels. Furthermore, there is a dearth of research on antioxidant hydrogels and the few reports of these materials focus on entrapping and releasing antioxidant compounds.[23] Our laboratory has previously described the synthesis and characterization of an intrinsically antioxidant thermoresponsive citrate-based hydrogel that can be safely resorbed by the body.[24] Specifically, poly(polyethyleneglycol citrate-co-*N*-isopropylacrylamide (PPCN) is a liquid at room temperature (22°C) and has a lower critical solution temperature (LCST) between 26°C and 28°C depending on the medium, making it an interesting candidate material for entrapping HKUST-1 NPs under mild conditions for wound dressing applications. HKUST-1 was chosen as the model MOFs because of its easy and scalable synthesis and the reported low toxicity of the ligand H_3BTC (LD50: 8.4 g/kg in rats).[25]

Herein, we describe the synthesis and characterization of a novel antioxidant HKUST-1-thermoresponsive polydiolcitrate hydrogel composite to accelerate chronic wound healing. We show that PPCN can stabilize HKUST-1 NPs in protein solution leading to slow release

of copper ions and the use of HKUST-1 does not affect PPCN's gelation properties. We also show that copper ion delivery through H-HKUST-1 results in reduced cytotoxicity and apoptosis, increased dermal cell migration *in vitro*, and enhanced wound healing in a splinted excisional wound healing diabetic mouse model.

2. Results and Discussion

2.1. PPCN-HKUST-1 interactions enable sustained copper ion release and maintain thermoresponsive and antioxidant properties

HKUST-1 NPs were obtained following the reaction between copper acetate monohydrate and 1,3,5-benzenetricarboxylic acid (H_3BTC) at room temperature for 20 min.[25b] PPCN was synthesized as previously described by us.[24] HKUST-1 NPs were added to a PPCN solution of 100 mg/mL, resulting in a homogeneous dispersion (H-HKUST-1). Given the literature describing the use of $CuSO_4$ in wound healing applications, $CuSO_4$ was added to PPCN to create a copper ion-containing hydrogel (H-$CuSO_4$) to assess the impact of packaging copper ions in the MOFs. ^{1}H NMR analysis showed the characteristic peaks for PPCN at 3.77 ppm (N-CH- from *N*-isopropylacrylamide monomer (NIPAM)), 3.29–3.58 ppm (-CH_2CH_2O- from poly(ethylene glycol) (PEG)), and 0.97 ppm (-CH_3 from NIPAM) (Figure S1A). The characteristic peaks at 8.47 ppm could be assigned to aromatic C-H from the HKUST-1 (Figure S1B). For H-$CuSO_4$, characteristic peaks can be observed at 3.81 ppm, 3.30–3.60 ppm, and 1.02 ppm, which were similar to those of PPCN (Figure S1C). Both characteristic peaks for PPCN and HKUST-1 can be observed for H-HKUST-1 (Figure S1D). These results confirm that PPCN, HKUST-1 NPs and H-HKUST-1 were successfully prepared. Fourier Transform Infrared Spectroscopy (FTIR) analysis was performed to further confirm the successful preparation of H-HKUST-1. Both characteristic peaks for PPCN (3320 (NH amide), 2930, 2880 (CH_2, CH_3), 1650, 1560, 1390, 1370 (COO^-) cm^{-1}) and HKUST-1 (1650, 1560, 1450, 1380 (COO^-), 729 (benzene-ring), 490 (Cu-O) cm^{-1}) can be observed for H-HKUST-1, confirming the successful preparation of H-HKUST-1 (Figure S2D). Also, both characteristic peaks for PPCN and SO_4^{2-} (1130, 623 cm^{-1}) can be observed for H-$CuSO_4$, indicating H-$CuSO_4$ was successfully prepared (Figure S2C). According to dynamic light scattering (DLS), HKUST-1 NP size and polydispersity index (PDI) were 285.6 ± 2.7 nm and 0.16 ± 0.01, respectively (Figure S3). The zeta potential of HKUST-1 NPs was determined to be −4.9 ± 0.3 mV, which may reduce the ionic interactions between Cu^{2+} in the HKUST-1 and carboxyl groups in PPCN. Scanning electron microscopy (SEM) imaging confirmed the presence of HKUST-1 crystals within the hydrogel (Figure 1A). The addition of copper to PPCN in the form of HKUST-1 resulted in the sustained release of copper ions in phosphate-buffered saline (PBS) for approximately 24 hrs without any significant change in the PPCN gelation properties. H-$CuSO_4$ released 88.7% and 89.5% of loaded copper ions within 24 hrs in PBS and 10% fetal bovine serum (FBS), respectively (Figure 1B). In contrast, H-HKUST-1 released 56.5% and 61.5% of loaded copper ions within 24 hrs in PBS and 10% FBS, respectively (Figure 1B). The lower copper release amount from H-HKUST-1 may be due to the cooperative effect between HKUST-1 NPs and PPCN, meaning that HKUST-1 NPs did not interfere with PPCN gelation by shielding the positive charge of Cu^{2+} and PPCN hydrogel protected HKUST-1 NPs from degradation by limiting solvent access.

The LCSTs of PPCN and H-HKUST-1 were determined via rheology to be 28.1°C and 27.2°C, respectively (Figure 1C). However, the addition of an equivalent amount of copper ions in the form of $CuSO_4$ to PPCN resulted in partial gelation at room temperature (Figure 1D) and the destabilization of the thermoresponsive *N*-isopropylacrylamide groups as three crossover points between storage (G′) and loss (G″) moduli were detected at 26.0°C, 30.7°C, and 38.8°C (Figure 1C). These results suggest that Cu^{2+} in solution at those concentrations interfered with PPCN's gelation and prevented the formation of a stable hydrogel. This phenomenon was also observed when we tested the water soluble copper salts $CuCl_2$ and $Cu(NO_3)_2$. In contrast, $CuCO_3$, a sparingly soluble copper salt, did not promote PPCN gelation at room temperature (Figure S4A), possibly due to the low amount of copper ions in H-$CuCO_3$ (Figure S4B) and as a result less PPCN crosslinking for H-$CuCO_3$. The instability for H-$CuSO_4$ is possibly due to strong electrostatic interactions between copper ions and carboxyl groups in PPCN that create ionic crosslinks and hydrophobic islands of polyNIPAM within the network.[26] When PPCN, H-HKUST-1 and H-$CuSO_4$ were incubated at 37°C in 10% FBS, H-$CuSO_4$ was destabilized and disintegrated into small pieces while PPCN and H-HKUST-1 formed stable gels (Figure 1E). The mechanism of sol/gel transition likely involves hydrophobic interactions, hydrogen bonding, electrostatic interactions, and molecular chain movement.[27] For H-$CuSO_4$, the interaction between positively charged copper ions and negatively charged carboxylic acid may affect the formation of hydrogen bonds between water molecules and carboxyl groups in the gel. Also, electronic interactions may limit the molecular chain movement of PPCN, which would further influence the hydrophobic interactions between NIPAM in PPCN.[27] For H-HKUST-1, copper ions in HKUST-1 NPs are coordinated with the carboxyl groups of H_3BTC, minimizing interactions with the carboxyl groups in PPCN and reducing their effects on gelation. As a result, H-HKUST-1 forms a stable hydrogel with minimal impact on PPCN's original LCST.

The ability of H-HKUST-1 to scavenge the free radical cation, 2,2′-azino-bis(3-ethylbenzthiazoline-6-sulfonic acid) (ABTS) was assessed by determining the decrease in absorbance of ABTS. Both H-HKUST-1 and H-$CuSO_4$ exhibited rapid free radical scavenging activity as per ABTS assay with about 75% of radicals scavenged within 48 hrs. These results are similar to those obtained for PPCN, confirming that the antioxidant activity of PPCN is preserved after loading HKUST-1 NPs or $CuSO_4$ in PPCN.[24] For $CuSO_4$ and HKUST-1 NPs, the free radical scavenging activity over time was negligible, and comparable to the background signal obtained from ABTS in PBS (Figure 1F).

2.2. PPCN protects HKUST-1 NPs from degradation in protein-containing solution

The stability of HKUST-1 alone or dispersed in PPCN that was gelled at 37°C before and after incubation in 10% FBS was evaluated using transmission electron microscopy (TEM). HKUST-1 crystals were clearly visible before incubation in FBS and disintegrated after treatment with FBS, confirming that HKUST-1 is not stable in 10% FBS. However, HKUST-1 crystals in H-HKUST-1 were observed after treatment with FBS (Figure 1G), confirming that PPCN protected HKUST-1 from FBS-mediated disintegration, possibly through diffusion-limited degradation of HKUST-1 NPs.

X-ray diffraction (XRD) patterns were performed to detect the crystal structure and confirm the results of the TEM study. H-HKUST-1 exhibited obvious X-ray diffraction peaks, which were similar to HKUST-1 before treatment with 10% FBS. After treatment with 10% FBS, HKUST-1 peaks disappeared completely for HKUST-1 alone (Figure 1H). However, the characteristic peaks from HKUST-1 embedded in PPCN remained present at 4 hrs, further confirming that PPCN is able to stabilize HKUST-1 in protein-containing solution such as FBS by hindering their diffusion to the HKUST-1 NPs (Figure 1H).

2.3. HKUST-1 NPs are less toxic to cells when dispersed in PPCN

The cytotoxicity of $CuSO_4$, H-$CuSO_4$, HKUST-1 NPs and H-HKUST-1 toward human epithelial keratinocytes (HEKa) and human dermal fibroblasts (HDF) cells was evaluated using the 3-(4,5-dimethylthiazol-2-yl)-2,5-diphenyltetrazolium bromide (MTT) assay. The cytotoxicity of $CuSO_4$ increased with increasing concentrations and no obvious difference was observed after loading it into PPCN hydrogel. This is likely due to the fact that H-$CuSO_4$ breaks down in cell culture medium, suddenly releasing large amounts of copper ions (Figure 2A, B). The cytotoxicity of HKUST-1 NPs was comparable to that of $CuSO_4$, which may be due to the fact that HKUST-1 NPs are not stable in the cell culture medium, leading to a fast release of copper ions. However, H-HKUST-1 showed much lower toxicity against both HEKa and HDF cells, especially at high concentration (1 mM). This finding may be attributed to the sustained release of non-cytotoxic copper ion amounts from H-HKUST-1 (Figure 2A, B). PPCN and H_3BTC were not toxic to either cell type (Figure 2C, Figure S5).

2.4. H-HKUST-1 does not induce cell apoptosis

$CuSO_4$, H-$CuSO_4$ and HKUST-1 NPs induced 75.9 ± 3.2%, 84.4 ± 11.3% and 76.8 ± 12.4% cell apoptosis in HEKa cells, and 90.3 ± 6.5%, 91.1 ± 9.6% and 94.0 ± 8.0% cell apoptosis in HDF cells, respectively (Figure 2D). However, H-HKUST-1 only induced 10.7 ± 2.5% cell apoptosis in HEKa and 17.0 ± 5.4% cell apoptosis in HDF cells. As a reference, PBS induced 6.7 ± 2.2% in HEKa cells and 1.1 ± 0.2% in HDF cells and PPCN induced 8.6 ± 1.8% in HEKa cells and 7.3 ± 5.6% in HDF cells. These results are consistent with the lack of toxicity of H-HKUST-1, suggesting that H-HKUST-1 may be a suitable dressing material for chronic wound healing.

2.5. H-HKUST-1 promotes cell migration *in vitro*

The copper concentration that best stimulates cell migration with no cytotoxicity was determined via a scratch assay (Figure S6). For HEKa cells, $CuSO_4$ at 10 μM ($CuSO_4$-High) inhibited cell migration, whereas $CuSO_4$ at 1 μM ($CuSO_4$-Low) promoted cell migration (Figure S6Aa, B). For HDF cells, $CuSO_4$-High did not affect their migration when compared to non-treated cells. Cells treated with $CuSO_4$-Low had increased cell migration relative to those treated with $CuSO_4$-High at 54 hrs (Figure S6Ab, C). Therefore, a copper ion concentration of 1 μM was chosen for all subsequent experiments. The effect of PPCN, $CuSO_4$, H-$CuSO_4$, HKUST-1 NPs and H-HKUST-1 on cell migration was evaluated (Figure 3). The blank with the addition of the same volume of PBS (20 μL) was used as control. H_3BTC and PPCN-H_3BTC (H-H_3BTC) at the expected organic ligand concentration present in the HKUST-1 NPs were also tested as controls to confirm that any observed increase in

cell migration was due to Cu^{2+} (Figure S7). For HEKa cells, PPCN showed no obvious effect on cell migration at 8 hrs when compared to the blank. However, at non-cytotoxic concentrations, cells in wells exposed to $CuSO_4$ and H-$CuSO_4$ showed a significant increase in cell migration and this effect was enhanced in cells that were exposed to HKUST-1 NPs and H-HKUST-1. After incubation for 30 hrs, cells exposed to H-HKUST-1 showed the highest migration (91.7 ± 3.5%), followed by those exposed to HKUST-1 NPs (71.8 ± 10.2%), H-$CuSO_4$ (59.1 ± 8.6%), $CuSO_4$ (56.7 ± 12.6%) and PPCN (46.3 ± 7.7%) (Figure 3Aa, B). HDF cells exposed to PPCN, $CuSO_4$, H-$CuSO_4$, HKUST-1 NPs and H-HKUST-1 showed similar trends to those observed with HEKa cells. At 54 hrs after treatment, cells exposed to H-HKUST-1 exhibited the highest migration (71.4 ± 3.8%), compared to those exposed to HKUST-1 NPs (51.7 ±4.3%), H-$CuSO_4$ (32.7 ± 10.9%), $CuSO_4$ (34.2 ± 2.8%) and PPCN (27.2 ± 8.0%) (Figure 3Ab, C). H_3BTC and H-H_3BTC did not affect cell migration for either cell type (Figure S7).

The increased cell migration rates for cells exposed to $CuSO_4$, H-$CuSO_4$, HKUST-1 NPs and H-HKUST-1 are due to the presence of copper ions at low but potentially physiologically relevant concentration without obvious cytotoxicity. The application of $CuSO_4$ has been reported to stimulate the migration of keratinocytes and fibroblasts through inducing the expression of growth factors VEGF, bFGF and PDGF.[28] In our study, $CuSO_4$, H-$CuSO_4$, HKUST-1 NPs and H-HKUST-1 increased cell migration rates relative to the control groups. The comparable migration rates of cells exposed to H-$CuSO_4$ and $CuSO_4$ may be due to similar burst release of Cu^{2+} in both systems. H-HKUST-1 promoted the highest rate of cell migration in both cell types, probably because of the combination of free radical scavenging activity, lower cytotoxicity, and lower rate of apoptosis provided by the presence of the PPCN.

2.6. H-HKUST-1 promotes dermal wound healing in diabetic mice

The splinted excisional dermal wound model in mice was used to assess the efficacy and biocompatibility of H-HKUST-1 because it is a validated and widely used model to evaluate treatments to heal wounds.[29] Also, this model is reproducible, readily available, low cost, and relatively easy to implement. Wound contraction is minimized with the use of a splint allowing one to evaluate tissue regeneration in the wound.[30] Though excisional models in other species such as the rabbit ear dermal ulcer model have been developed to more closely mimic human wound healing, these models are not widely used because of the cost and lack of reagents for the species.[12a, 12b, 12d, 30] Generally, the upper bound of wound healing time increases with increasing wound size with 3 mm, 6 mm, and 10 mm non-splinted wounds healing in 12, 21, and 35 days, respectively.[29d, 31] A 6 mm splinted wound was chosen because it has been successfully used for drug efficacy evaluation.[29e, 30]

In this study, each mouse received two wounds and animals were randomly divided into two groups. Group one consisted of animals where one wound was treated with PBS and the other with HKUST-1 NPs in PBS. Group two consisted of animals where one wound was treated with PPCN and the other with H-HKUST-1. The mean blood glucose concentration was 290 ± 9 mg/dL at the beginning of the study and 310 ± 13 mg/dL at the end, confirming that the mice were diabetic during the wound-healing period. Wounds treated with H-

HKUST-1 were almost completely healed by day 21 whereas wounds treated with PBS, PPCN, and HKUST-1 NPs healed by day 39, 39 and 37 on average, respectively (Figure 4A). The quantitative analysis of digital images of wounds over time also showed that wounds treated with H-HKUST-1 healed significantly faster than those treated with PBS, PPCN and HKUST-1 NPs, especially at day 7, 14, 21, and 29 (Figure 4B). Wound closure rates for wounds treated with PBS, PPCN and HKUST-1 NPs were similar. The closure rates of wounds treated with H_3BTC and H-H_3BTC were comparable to those of wounds treated with PBS (Figure S8). The ability of H-HKUST-1 to stimulate wound healing *in vivo* is attributed to the sustained release of non-cytotoxic amounts of copper ions, which induced angiogenesis, collagen deposition and re-epithelialization during wound healing.[32] Also, the low toxicity and antioxidant moist environment provided by the PPCN component of H-KKUST-1 likely contributed to the increased wound closure rate. The copper content in H-HKUST-1 remaining on the wounds was determined at day 7. Less than 0.1% of copper was left in H-HKUST-1. Therefore, over 99.9% of the entrapped copper was released into the wound. The body weight of mice treated with PPCN and H-HKUST-1 remained constant throughout the study whereas the body weight of animals treated with PBS and HKUST-1 NPs decreased significantly by the end of the study (Figure 4C). These findings further confirm that PPCN and H-HKUST-1 are significantly less toxic than HKUST-1 NPs. Interestingly, wounds treated with HKUST-1 NPs showed wound enlargement relative to those treated with PBS, PPCN and H-HKUST-1 at day 4, possibly due to toxicity of HKUST-1 NPs, which are unstable and release a large amount of copper ions within a short time.

2.7. H-HKUST-1 promotes angiogenesis and collagen deposition

Diminished peripheral blood flow and decreased local neovascularization are critical factors that contribute to delayed wound healing in patients with diabetes.[33] Furthermore, activation of angiogenesis is required to sustain newly formed granulation tissue.[34] Therefore, the correction of impaired local angiogenesis should be a key component of therapeutic protocols for the treatment of chronic wounds of the lower extremities and diabetic foot ulcers.[35] Optical coherence tomograph angiography (OCTA) was used to investigate neovascularization at the site of injury after treatment. OCTA is a non-invasive optical technique that images the microvasculature by harnessing the motion contrast of the red blood cells.[36] OCTA showed that H-HKUST-1 and HKUST-1 NPs promoted the formation of a more stable and densely perfused vascular network at the wound site when compared to PBS and PPCN (Figure 5A). The blood vessels in healed skin were also observed via histology, specifically hematoxyin and eosin (H&E) staining. Neovascularization, including blood vessel number and area, was markedly increased in HKUST-1- and H-HKUST-1-treated wounds (Figure 5B). Histomorphometry revealed that the blood vessel number within the granulation tissue was almost 4- and 5-fold higher in HKUST-1- and H-HKUST-1-treated wounds, respectively, than that in the PBS-treated wounds (Figure 5C). Mean microvessel densities in HKUST-1- and H-HKUST-1-treated wounds were 44.4 ± 5.2 and 54.0 ± 14.4 vessels/mm^2, respectively, whereas microvessel densities in PBS- and PPCN-treated wounds were 11.3 ± 8.0 and 18.3 ± 6.9 vessels/mm^2, respectively. The capacity of HKUST-1 NPs and H-HKUST-1 to stimulate new blood vessel formation is attributed to Cu^{2+}, which has been reported to increase the expression of

angiogenic genes for VEGF, bFGF and PDGF.[5a] The promotion of angiogenesis likely allowed an adequate supply of oxygen and nutrients as well as accelerated migration of the requisite cells and humoral factors into the wounds. These processes, in turn, are believed to facilitate the formation of granulation tissue and collagen synthesis, leading to improved wound healing.[32]

The synthesis and deposition of collagen is also a critical process in wound healing. As a cofactor to lysyl oxidase, Cu^{2+} stimulates the expression of matrix metalloproteinase-2 and collagen in fibroblasts, enhancing wound healing.[32] Masson's trichrome staining showed significantly more collagen and a smaller granulation tissue gap width remaining in the wounds treated with HKUST-1 NPs and H-HKUST-1 than in wounds treated with PBS and PPCN. When compared to wounds treated with HKUST-1, the H-HKUST-1-treated wounds exhibited a smaller granulation tissue gap width (Figure 5D, E). These results show that although both HKUST-1 NPs and H-HKUST-1 promoted collagen deposition in the granulation tissue, H-HKUST-1 exhibited the highest impact on the maturation of granulation tissue and regeneration of the epidermis. HEKa cells, one of the major cellular components of the epidermis, are important to the re-epithelialization process in dermal wounds.[37] H-HKUST-1 promoted the migration of HEKa cells and provided a moist environment that facilitated re-epithelialization at the wound site.[38]

3. Conclusions

To summarize, a novel H-HKUST-1 composite has been prepared successfully and a cooperative, stabilizing effect has been demonstrated between HKUST-1 NPs and PPCN. In effect, HKUST-1 NPs did not destabilize the PPCN gel network by shielding positive charges of stored Cu^{2+} and PPCN protected HKUST-1 NPs from disintegration possibly through diffusion-limited degradation. Moreover, H-HKUST-1 enabled the sustained release of copper ions while preserving the antioxidant properties of PPCN, which reduced the cytotoxicity of copper ions and promoted cell migration, angiogenesis, collagen deposition, and accelerated wound healing in diabetic mice. H-HKUST-1 provides a new approach to locally deliver copper ions efficiently and may potentially be useful as a novel dressing for the treatment of chronic non-healing wounds.

4. Experimental Section

Materials, cell lines and animals

Copper acetate monohydrate and H_3BTC were purchased from Alfa Aesar (Ward Hill, MA). Citric acid, PEG, glycerol 1,3-diglycerolate diacrylate, 2,2-Azobisisobutyronitrile (AIBN), NIPAM, and MTT were obtained from Sigma-Aldrich (St. Louis, MO). All the other reagents were of analytical grade. HEKa cells were purchased from Lonza and cultured with keratinocyte growth media (KGM) (Lonza, Walkersville, MD). HDF cells were obtained from Life technologies (Grand Island, NY) and cultured in Dulbecco's Modified Eagle's Medium (DMEM) containing 10% FBS, 100 Unit/mL penicillin G sodium, and 100 μg/mL streptomycin sulfate. All cells were maintained at 37°C in a humidified and 5% CO_2 incubator. Diabetic (db/db) mutant mice (BKS.Cg-*m* $^{+/+}$ *Leprdb*, #000642; Homozygous for $Lepr^{db}$) were purchased from Jackson Laboratory (Bar Harbor, Maine). Protocols described

in this study were approved by Institutional Animal Care and Use Committee (IACUC) of Northwestern University.

Preparation and characterization of H-HKUST-1

PPCN was synthesized by our group as reported previously.[24] Firstly, poly (polyethyleneglycol citrate) acrylate prepolymer (PPCac) was prepared with citric acid, PEG and glycerol 1,3-diglycerolate diacrylate through polycondensation reaction. Subsequently, PPCac was reacted with pre-purified NIPAM overnight through free radical polymerization using AIBN as the free radical initiator. The reaction product, PPCN, was obtained by precipitation and purification with diethyl ether. The obtained PPCN was then dissolved in PBS, neutralized to pH 7.4 with sodium hydroxide and stored as a lyophilized powder for further use. ^{1}H NMR (400 MHz, DMSO-d_6/D_2SO_4 (9/1, v/v), δ): 4.00–4.13 (-OCH_2-), 3.77 (N-CH-), 3.29–3.58 (-OCH_2CH_2O-), 2.60–2.78 (O=C-CH_2-), 0.97 (-CH_3) (Figure S1A); FTIR (KBr): ν = 3430 (ν(OH) H_2O), 3320 (ν(NH) *amide*), 2930 (ν_{as}(CH) *CH_2*, *CH_3*), 2880 (ν_s(CH) *CH_2*, *CH_3*), 1650 (ν(C=O) *amide I*, ν_{as}(COO^-)), 1540 (ν_{as}(COO^-)), 1390, 1370 (ν_s(COO^-)), 1130 (ν(C-O)) cm^{-1} (Figure S2A); Yield: 75%–86%; ^{1}H NMR and FTIR spectroscopy of PPCN prepared for this study are comparable to those previously published by us.[24]

HKUST-1 NPs were synthesized according to a previously reported method.[25b] Briefly, copper acetate monohydrate (0.15 g, 0.75 mmol) dissolved in distilled water (2 mL) was dropwise added to H_3BTC (0.11 g, 0.5 mmol) dissolved in ethanol (2 mL), followed by stirring at room temperature for 20 min to form gel-like dark turquoise suspension. The suspension was then centrifuged and the precipitate was washed with ethanol/water (1:1, v/v) solution twice to obtain purified HKUST-1. ^{1}H NMR (400 MHz, DMSO-d_6/D_2SO_4 (9/1, v/v) δ): 8.47 (s, 3H, Ar H) (Figure S1B); FTIR (KBr): ν = 1620, 1560 (ν_{as}(COO^-)), 1440, 1380 (ν_s(COO^-)), 1110 (δ(Aromatic C–H) ip), 941 (δ(Aromatic C–H) oop), 729 (ν(C=C) benzene-ring oop), 490 (ν(Cu-O)) cm^{-1} (Figure S2B); Yield: 99.5%; ^{1}H NMR and FTIR spectra of HKUST-1 are comparable to previously published results.[39]

H-HKUST-1 was prepared by adding HKUST-1 NPs to PPCN solution (100 mg/mL) to a copper concentration of 0.1 M under vortex at room temperature. ^{1}H NMR (400 MHz, DMSO-d_6/D_2SO_4 (9/1, v/v), δ): 8.51 (s, Ar H), 3.89–4.12 (-OCH_2-), 3.79 (N-CH-), 3.08–3.50 (-OCH_2CH_2O-), 0.91 (-CH_3) (Figure S1D); FTIR (KBr): ν = 3430 (ν(OH) H_2O), 3320 (ν(NH) *amide*), 2930 (ν_{as}(CH) *CH_2*, *CH_3*), 2880 (ν_s(CH) *CH_2*, *CH_3*), 1650 (ν(C=O) *amide I*, ν_{as}(COO^-)), 1560 (ν_{as}(COO^-)), 1450, 1380 (ν_s(COO^-)), 1110 (δ(Aromatic C–H) ip), 951 (δ(Aromatic C–H) oop), 729 (ν(C=C) benzene-ring oop), 490 (ν(Cu-O)) cm^{-1} (Figure S2D); ^{1}H NMR and FTIR spectra are comparable to previously published results.[24, 39a] As controls, $CuSO_4$-loaded PPCN hydrogel (H-$CuSO_4$) was also prepared using the same procedure. ^{1}H NMR (400 MHz, DMSO-d_6/D_2SO_4 (9/1, v/v), δ): 4.06–4.14 (-OCH_2-), 3.81 (N-CH-), 3.30–3.60 (-OCH_2CH_2O-), 2.60–2.80 (O=C-CH_2-), 1.02 (-CH_3) (Figure S1C); FTIR (KBr): ν = 3430 (ν(OH) H_2O), 3320 (ν(NH) *amide*), 2930 (ν_{as}(CH) *CH_2*, *CH_3*), 2880 (ν_s(CH) *CH_2*, *CH_3*), 1650 (ν(C=O) *amide I*, ν_{as}(COO^-)), 1540 (ν_{as}(COO^-)), 1390, 1370 (ν_s(COO^-)), 1130 (ν(C-O), ν_{as}(SO_4^{2-})), 623 (ν_s(SO_4^{2-})) cm^{-1}.

The particle size and zeta potential of HKUST-1 NPs were determined by dynamic light scattering using a Zetasizer (Malvern, UK). The morphology of H-HKUST-1 was visualized using quick-freeze deep etch (QFDE) method as reported by our group.[24] H-HKUST-1 solution was placed directly on the QFDE specimen disks, heated at 45°C until solid, and slam frozen. After etching, an exact replica of exposed gel structure was made, coated with Pt (Thickness: 3.9 nm) and Carbon (Thickness: 3.1 nm), and examined using SEM.

The release of copper ions from H-HKUST-1 or H-$CuSO_4$ in 0.1 M PBS (pH 7.4, 37°C) or 10% FBS (pH 7.4, 37°C) was assessed. Briefly, H-HKUST-1 solution (80 μL) was added into tubes, allowed to solidify at 37°C for 5 min and gently rinsed with 0.1 M PBS (pH 7.4, 37°C). After that, samples were incubated in 5 mL PBS or 10% FBS and continuously shaken with a speed of 100 rpm at 37°C. At predetermined intervals, 1 mL of release media was taken out for content measurement and replenished with an equal volume of fresh media at 37°C. The amount of the released copper was measured by inductively coupled plasma mass spectrometry (ICP-MS). H-$CuCO_3$ was prepared by adding $CuCO_3$ to PPCN solution (100 mg/mL) to achieve a copper concentration of 0.1 M under vortex at room temperature. The release of copper ions from $CuCO_3$ and H-$CuCO_3$ was also determined as described above.

The stability of PPCN after loading HKUST-1 NPs was investigated by observing morphological changes upon the addition of HKUST-1 NPs at room temperature and after treatment with 10% FBS at 37°C, respectively. The rheology of H-HKUST-1 was determined by discovery hybrid rheometers (TA Instruments). The storage (elastic) modulus G′ and loss (viscous) modulus G″ versus temperature were measured between 20°C and 40°C using a constant heating rate of 2°C/min. The temperature at the cross point of G′ and G″ was defined as gelation temperature.

The ability of H-HKUST-1 to scavenge the free radical cation, ABTS, was assessed. A stock solution of 7 mM ABTS and 2.45 mM sodium persulfate in MQ water was prepared and left overnight in the dark at room temperature, after which the solution was sequentially filtered with 0.45 μm filter. This working solution (1 mL) was then exposed to 1 mL of samples (PBS, $CuSO_4$, HKUST-1, PPCN, H-$CuSO_4$, H-HKUST-1; Cu: 0.5 μM; PPCN: 50 mg/mL) and incubated at 37 °C. At each time point, ABTS solution was sampled, diluted with MQ water (1:8) and the absorbance was measured at 734 nm. All measurements were performed in triplicate. The antiradical activity was measured as % inhibition of free radicals by measuring the decrease in absorbance taking into account changes due to ABTS in PBS at different time points as the absorbance of ABTS in PBS can slowly decrease overtime.

Stability of HKUST-1 NPs in PPCN when exposed to a protein solution

H-HKUST-1 gel was treated with 10% FBS at 37 °C for 1 hr, centrifuged at 4°C for 5 min at the speed of 10,000 rpm, washed twice with ice cold water and resuspended with 50% ethanol. Thereafter, the morphology of H-HKUST-1 was observed with TEM. HKUST-1 with the same treatment was used as control. After treatment with 10% FBS at 37°C for 1 hr and 4 hrs, H-HKUST-1 gels were frozen with liquid nitrogen and dried with freeze dryer overnight. The crystalline form of H-HKUST-1 was determined by X-ray diffraction. HKUST-1 NPs with the same treatment were used as control.

Cytotoxicity assay

HEKa and HDF cells seeded in 96-well plates (5×10^3 cells/well) were incubated with a series of concentrations of PPCN, H_3BTC, $CuSO_4$, H-$CuSO_4$, HKUST-1 NPs or H-HKUST-1 for 48 hrs. Then, MTT solution was added to each well to a concentration of 0.5 mg/mL and incubated for an additional 4 hrs. After that, the medium was removed and 100 μL of dimethyl sulfoxide was added to dissolve crystals formed by living cells. Absorbance at 570 nm was measured using a microplate reader. Cell viability was expressed as a percentage of the absorbance to that of the control experiment without treatment.

Apoptosis assay

HEKa and HDF cells seeded in 12-well plates (4×10^4 cells/well) were incubated with PPCN, $CuSO_4$, H-$CuSO_4$, HKUST-1 NPs or H-HKUST-1 (Cu: 0.5 mM) for 24 hrs. Cells were harvested, washed twice with ice-cold PBS, stained with Alexa Fluor 488 conjugated Annexin V and PI for 15 min at room temperature in dark, and then analyzed by flow cytometry.

Scratch assay

HEKa and HDF cells were seeded in 24-well plates (2×10^4 cells/well) and allowed to form a confluent monolayer. After starvation with FBS-free medium for 24 hrs, the cell monolayer was scratched in a straight-line using a 200 μL pipette tip to mimic an incisional wound. Cells were then washed with PBS to remove cell debris, treated with $CuSO_4$ at two different concentrations (Cu: 10 and 1 μM) and incubated at 37°C with the medium containing 1% FBS. At desired time intervals, cells were photographed and cell migration rate was calculated using the formula shown below:

$$\%\,\text{Cell migration} = \frac{\text{A0} - \text{At}}{\text{A0}} \times 100$$

A0: The scratch area at 0 h;

At: The scratch area without cell migration at different time points

After that, new 24-well plates were seeded and cells were treated with PPCN, $CuSO_4$, H-$CuSO_4$, HKUST-1 NPs or H-HKUST-1 at a copper concentration of 1 μM. The % cell migration was determined as shown above. Cell migration experiments were also perfomed in the presence of H_3BTC, H-H_3BTC, $CuCO_3$ and H-$CuCO_3$.

Wound healing in vivo

The mice, 8 – 10 weeks of age, were anesthetized with isoflurane and the hair on their backs was shaved and completely removed with depilatory cream. After disinfection with betadine and alcohol swabs, mice were subcutaneously injected with buprenorphine (0.5 mg/kg) and two wounds were gently outlined by a marked 6 mm punch biopsy (Acuderm, Fort Lauderdale, FL) on each side of the mouse. Following the outline, full-thickness wounds were made using a McPherson-Vannas Micro Scissor (World Precision Instruments, Sarasota, FL) and fixed with sterilized and donut-shaped splints. The mice were randomly divided into two groups (n = 6). Animals where one wound was treated with PBS (40 μL)

and the other with HKUST-1 (Cu: 1 mM, 40 μL) and animals where one wound was treated with PPCN (100 mg/mL, 40 μL) and the other with H-HKUST-1 (Cu: 1 mM, PPCN: 100 mg/mL, 40 μL). To control for the effects that the other components of HKUST-1 may have on wound healing, wound closure experiments were performed with animals where one wound was treated with H_3BTC and the other with H-H_3BTC (H_3BTC: 0.67 mM, PPCN: 100 mg/mL, 40 μL). Wounds were covered with Tegaderm and coban, animals were individually caged, and the various treatments were reapplied twice a week in the first two weeks and once a week after two weeks. H-HKUST-1 and PPCN hydrogel remaining in the wounds were collected before reapplying samples and digested by concentrated HNO_3 overnight. The copper concentration was determined by ICP-MS. The *in vivo* release was calculated as follows:

$$\%\,\text{Copper release} = \frac{W_0 - (W_1 - W_2)}{W_0} \times 100$$

W_0: Initial copper content of H-HKUST-1 applied to the wounds;

W_1: Copper content of H-HKUST-1 hydrogel remaining in the wounds;

W_2: Endogenous copper content in PPCN hydrogel remaining in the wounds.

In addition, the mice were weighed once a week during the experiment and the blood glucose concentration was randomly monitored at the beginning and at the end time point. Wounds were photographed with digital camera, wound pixel area was calculated with Image J and normalized to the fixed inner area of the splint. The wound closure was calculated with a formula as below:

$$\%\,\text{Wound closure} = \left(1 - \frac{\left(\frac{\text{wound area}}{\text{splint area}}\right)\ \text{Day x}}{\left(\frac{\text{wound area}}{\text{splint area}}\right)\ \text{Day 0}}\right) \times 100$$

The vascular network within the wound site was visualized to assess angiogenesis at the wound site. The vessel contrast was enhanced using the non-invasive, label-free OCTA technique. Briefly, each B-scan location was repeatedly scanned for five-times to capture the dynamic scattering resulted from the moving blood cells within the vessel. High-pass filtering was applied among these five-consecutive B-scans to enhance blood vessel contrast, while suppressing signals from other static tissue. After automated image segmentation that removes excess reflection from the air-skin interface, image stacks were integrated along depth-direction to generate en face OCT angiography.[36]

Histopathological analysis

The whole wound tissue with a margin of around 2 mm of ambient unwounded skin was excised at the end time point, fixed with 4% paraformaldehyde for 24 hrs, embedded in paraffin, and sectioned into 7 μm thickness slices for H&E and Masson's trichrome staining. The development of neovascularization, epidermis, granulation tissue and collagen deposition were inspected.

Supplementary Material

Refer to Web version on PubMed Central for supplementary material.

Acknowledgments

Research reported in this publication was supported, in part, by the National Institutes of Health's National Center for Advancing Translational Sciences, Grant Number UL1TR000150. The content is solely the responsibility of the authors and does not necessarily represent the official views of the National Institutes of Health. SEM samples were prepared with Leica EM-PACT2 (purchased with the support of NCRR 1S10RR022494) and Cressington CFE-60 QFDE Unit (purchased with the support of NCRR S10 RR16701). Zetasizer, SEM and FT-IR measurements were performed in EPIC and Keck-II facilities of the NUANCE Center at Northwestern University, with the support from Soft and Hybrid Nanotechnology Experimental (SHyNE) Resource (NSF NNCI-1542205); MRSEC program (NSF DMR-1121262) at the Materials Research Center; the International Institute for Nanotechnology (IIN); the Keck Foundation; and the State of Illinois, through the IIN.

References

1. a Randeria PS, Seeger MA, Wang XQ, Wilson H, Shipp D, Mirkin CA, Paller AS. Proc Natl Acad Sci U S A. 2015; 112:5573–5578. [PubMed: 25902507] b Mudge EJ. Int Wound J. 2015; 12:4–9. [PubMed: 24618286] c Augustin M, Herberger K, Kroeger K, Muenter KC, Goepel L, Rychlik R. Int Wound J. 2014
2. Centers for Disease Control and Prevention. National Diabetes Statistics Report: Estimates of Diabetes and Its Burden in the United States, 2014. Atlanta, GA: U.S. Department of Health and Human Services; 2014.
3. a Randeria PS, Seeger MA, Wang XQ, Wilson H, Shipp D, Mirkin CA, Paller AS. Proc Natl Acad Sci U S A. 2015; 112:5573–5578. [PubMed: 25902507] b Nakamura Y, Ishikawa H, Kawai K, Tabata Y, Suzuki S. Biomaterials. 2013; 34:9393–9400. [PubMed: 24054847]
4. a Dreifke MB, Jayasuriya AA, Jayasuriya AC. Mater Sci Eng C Mater Biol Appl. 2015; 48:651–662. [PubMed: 25579968] b Nuschke A. Organogenesis. 2014; 10:29–37. [PubMed: 24322872]
5. a Dioufa N, Schally AV, Chatzistamou I, Moustou E, Block NL, Owens GK, Papavassiliou AG, Kiaris H. Proc Natl Acad Sci U S A. 2010; 107:18611–18615. [PubMed: 20937882] b Sun G, Zhang X, Shen YI, Sebastian R, Dickinson LE, Fox-Talbot K, Reinblatt M, Steenbergen C, Harmon JW, Gerecht S. Proc Natl Acad Sci U S A. 2011; 108:20976–20981. [PubMed: 22171002] c Pina S, Oliveira JM, Reis RL. Adv Mater. 2015; 27:1143–1169. [PubMed: 25580589] d Loomba L, Scarabelli T. Ther Deliv. 2013; 4:1179–1196. [PubMed: 24024515] e Chen WY, Chang HY, Lu JK, Huang YC, Harroun SG, Tseng YT, Li YJ, Huang CC, Chang HT. Adv Funct Mater. 2015:n/a–n/a.
6. Gopal A, Kant V, Gopalakrishnan A, Tandan SK, Kumar D. Eur J Pharmacol. 2014; 731:8–19. [PubMed: 24632085]
7. Mandinov L, Mandinova A, Kyurkchiev S, Kyurkchiev D, Kehayov I, Kolev V, Soldi R, Bagala C, de Muinck ED, Lindner V, Post MJ, Simons M, Bellum S, Prudovsky I, Maciag T. Proc Natl Acad Sci U S A. 2003; 100:6700–6705. [PubMed: 12754378]
8. a Marelli B, Le Nihouannen D, Hacking SA, Tran S, Li J, Murshed M, Doillon CJ, Ghezzi CE, Zhang YL, Nazhat SN, Barralet JE. Biomaterials. 2015; 54:126–135. [PubMed: 25907046] b Gillespie JM. Australas J Dermatol. 1973; 14:127–131. [PubMed: 4793759]
9. a Amna T, Hassan MS, Yang J, Khil MS, Song KD, Oh JD, Hwang I. Int J Nanomedicine. 2014; 9:891–898. [PubMed: 24611006] b Borkow G, Gabbay J, Dardik R, Eidelman AI, Lavie Y, Grunfeld Y, Ikher S, Huszar M, Zatcoff RC, Marikovsky M. Wound Repair Regen. 2010; 18:266–275. [PubMed: 20409151] c Sen CK, Khanna S, Venojarvi M, Trikha P, Ellison EC, Hunt TK, Roy S. Am J Physiol. 2002; 282:H1821–1827.
10. a Guo L, Panderi I, Yan DD, Szulak K, Li Y, Chen YT, Ma H, Niesen DB, Seeram N, Ahmed A, Yan B, Pantazatos D, Lu W. ACS nano. 2013; 7:8780–8793. [PubMed: 24053214] b Hanagata N, Zhuang F, Connolly S, Li J, Ogawa N, Xu M. ACS nano. 2011; 5:9326–9338. [PubMed: 22077320]
11. Chen Z, Meng H, Xing G, Chen C, Zhao Y, Jia G, Wang T, Yuan H, Ye C, Zhao F, Chai Z, Zhu C, Fang X, Ma B, Wan L. Toxicology letters. 2006; 163:109–120. [PubMed: 16289865]

12. a Xu XX, Nie FL, Wang YB, Zhang JX, Zheng W, Li L, Zheng YF. Acta biomaterialia. 2012; 8:886–896. [PubMed: 22040688] b Ramakrishnan R, BB, Aprem AS. Contraception. 2015; 92:585–588. [PubMed: 26363430] c Alvarez F, Schilardi PL, de Mele MF. Contraception. 2012; 85:91–98. [PubMed: 22067791] d Xu XX, Ding MH, Zhang JX, Zheng W, Li L, Zheng YF. Journal of biomedical materials research Part B, Applied biomaterials. 2013; 101:1428–1436.
13. a Zhuang JL, Ceglarek D, Pethuraj S, Terfort A. Adv Funct Mater. 2011; 21:1442–1447.b Majano G, Martin O, Hammes M, Smeets S, Baerlocher C, Pérez-Ramírez J. Adv Funct Mater. 2014; 24:3837–3837.
14. Lu W, Wei Z, Gu ZY, Liu TF, Park J, Park J, Tian J, Zhang M, Zhang Q, Gentle T 3rd, Bosch M, Zhou HC. Chem Soc Rev. 2014; 43:5561–5593. [PubMed: 24604071]
15. Mason JA, Oktawiec J, Taylor MK, Hudson MR, Rodriguez J, Bachman JE, Gonzalez MI, Cervellino A, Guagliardi A, Brown CM, Llewellyn PL, Masciocchi N, Long JR. Nature. 2015; 527:357–361. [PubMed: 26503057]
16. Zhang W, Lu G, Cui C, Liu Y, Li S, Yan W, Xing C, Chi YR, Yang Y, Huo F. Adv Mater. 2014; 26:4056–4060. [PubMed: 24710716]
17. Guo Y, Feng X, Han T, Wang S, Lin Z, Dong Y, Wang B. J Am Chem Soc. 2014; 136:15485–15488. [PubMed: 25325884]
18. Hu Z, Deibert BJ, Li J. Chem Soc Rev. 2014; 43:5815–5840. [PubMed: 24577142]
19. Okawa H, Sadakiyo M, Yamada T, Maesato M, Ohba M, Kitagawa H. J Am Chem Soc. 2013; 135:2256–2262. [PubMed: 23301940]
20. a Horcajada P, Chalati T, Serre C, Gillet B, Sebrie C, Baati T, Eubank JF, Heurtaux D, Clayette P, Kreuz C, Chang JS, Hwang YK, Marsaud V, Bories PN, Cynober L, Gil S, Ferey G, Couvreur P, Gref R. Nat Mater. 2010; 9:172–178. [PubMed: 20010827] b Atmaja B, Lui BH, Hu Y, Beck SE, Frank CW, Cochran JR. Adv Funct Mater. 2010; 20:4091–4097. [PubMed: 25750609] c Suresh VM, George SJ, Maji TK. Adv Funct Mater. 2013; 23:5585–5590.d Wu P, Wang J, He C, Zhang X, Wang Y, Liu T, Duan C. Adv Funct Mater. 2012; 22:1698–1703.e He C, Liu D, Lin W. Chem Rev. 2015; 115:11079–11108. [PubMed: 26312730]
21. Della Rocca J, Liu D, Lin W. Acc Chem Res. 2011; 44:957–968. [PubMed: 21648429]
22. Zhang W, Hu Y, Ge J, Jiang HL, Yu SH. J Am Chem Soc. 2014; 136:16978–16981. [PubMed: 25412280]
23. Li J, Shu Y, Hao T, Wang Y, Qian Y, Duan C, Sun H, Lin Q, Wang C. Biomaterials. 2013; 34:9071–9081. [PubMed: 24001992]
24. Yang J, van Lith R, Baler K, Hoshi RA, Ameer GA. Biomacromolecules. 2014; 15:3942–3952. [PubMed: 25295411]
25. a Farrusseng, D. WILEY-VCH; 2011. p. 217b Xiao B, Yuan Q, Williams RA. Chem Commun. 2013; 49:8208–8210.
26. a Kim GO, Kim N, Kim da Y, Kwon JS, Min BH. Molecules (Basel, Switzerland). 2012; 17:13704–13711.b Burba CM, Carter SM, Meyer KJ, Rice CV. The journal of physical chemistry B. 2008; 112:10399–10404. [PubMed: 18681469]
27. Cheng YH, Yang SH, Su WY, Chen YC, Yang KC, Cheng WT, Wu SC, Lin FH. Tissue Eng Part A. 2010; 16:695–703. [PubMed: 19769528]
28. Sousa JE, Serruys PW, Costa MA. Circulation. 2003; 107:2274–2279. [PubMed: 12732594]
29. a Sato H, Ebisawa K, Takanari K, Yagi S, Toriyama K, Yamawaki-Ogata A, Kamei Y. Annals of plastic surgery. 2015; 74:114–120. [PubMed: 25188249] b Maan ZN, Januszyk M, Rennert RC, Duscher D, Rodrigues M, Fujiwara T, Ho N, Whitmore A, Hu MS, Longaker MT, Gurtner GC. Plastic and reconstructive surgery. 2014; 134:402e–411e.c Zhang X, Yan X, Cheng L, Dai J, Wang C, Han P, Chai Y. PloS one. 2013; 8:e84548. [PubMed: 24376825] d Greives MR, Samra F, Pavlides SC, Blechman KM, Naylor SM, Woodrell CD, Cadacio C, Levine JP, Bancroft TA, Michalak M, Warren SM, Gold LI. Wound Repair Regen. 2012; 20:715–730. [PubMed: 22985041] e Fujita K, Kuge K, Ozawa N, Sahara S, Zaiki K, Nakaoji K, Hamada K, Takenaka Y, Tanahashi T, Tamai K, Kaneda Y, Maeda A. PloS one. 2015; 10:e0144166. [PubMed: 26657737]
30. Galiano RD, Michaels Jt, Dobryansky M, Levine JP, Gurtner GC. Wound Repair Regen. 2004; 12:485–492. [PubMed: 15260814]

31. a Zhao G, Usui ML, Underwood RA, Singh PK, James GA, Stewart PS, Fleckman P, Olerud JE. Wound Repair Regen. 2012; 20:342–352. [PubMed: 22564229] b Peng C, Chen B, Kao HK, Murphy G, Orgill DP, Guo L. Plastic and reconstructive surgery. 2011; 128:673e–684e.c Huang C, Orbay H, Tobita M, Miyamoto M, Tabata Y, Hyakusoku H, Mizuno H. Wound Repair Regen. 2015d Aijaz A, Faulknor R, Berthiaume F, Olabisi RM. Tissue Eng Part A. 2015; 21:2723–2732. [PubMed: 26239745] e Hsu I, Parkinson LG, Shen Y, Toro A, Brown T, Zhao H, Bleackley RC, Granville DJ. Cell death & disease. 2014; 5:e1458. [PubMed: 25299783] f Okizaki S, Ito Y, Hosono K, Oba K, Ohkubo H, Amano H, Shichiri M, Majima M. Biomedicine & pharmacotherapy = Biomedecine & pharmacotherapie. 2015; 70:317–325. [PubMed: 25677561] g Cheng CF, Sahu D, Tsen F, Zhao Z, Fan J, Kim R, Wang X, O'Brien K, Li Y, Kuang Y, Chen M, Woodley DT, Li W. The Journal of clinical investigation. 2011; 121:4348–4361. [PubMed: 22019588] h Ansurudeen I, Sunkari VG, Grunler J, Peters V, Schmitt CP, Catrina SB, Brismar K, Forsberg EA. Amino acids. 2012; 43:127–134. [PubMed: 22451275] i Cheng C, Singh V, Krishnan A, Kan M, Martinez JA, Zochodne DW. PloS one. 2013; 8:e75877. [PubMed: 24098736]

32. Zhao S, Li L, Wang H, Zhang Y, Cheng X, Zhou N, Rahaman MN, Liu Z, Huang W, Zhang C. Biomaterials. 2015; 53:379–391. [PubMed: 25890736]

33. Liu ZJ, Velazquez OC. Antioxid Redox Signal. 2008; 10:1869–1882. [PubMed: 18627349]

34. Ebrahimian TG, Pouzoulet F, Squiban C, Buard V, Andre M, Cousin B, Gourmelon P, Benderitter M, Casteilla L, Tamarat R. Arterioscler Thromb Vasc Biol. 2009; 29:503–510. [PubMed: 19201690]

35. Eming SA, Martin P, Tomic-Canic M. Sci Transl Med. 2014; 6:265sr266.

36. Yi J, Chen S, Backman V, Zhang HF. Biomed Opt Express. 2014; 5:3603–3612. [PubMed: 25360376]

37. Pastar I, Stojadinovic O, Yin NC, Ramirez H, Nusbaum AG, Sawaya A, Patel SB, Khalid L, Isseroff RR, Tomic-Canic M. Adv Wound Care. 2014; 3:445–464.

38. Sood A, Granick MS, Tomaselli NL. Adv Wound Care. 2014; 3:511–529.

39. a Kim HK, Yun WS, Kim MB, Kim JY, Bae YS, Lee J, Jeong NC. J Am Chem Soc. 2015; 137:10009–10015. [PubMed: 26197386] b Zybaylo O, Shekhah O, Wang H, Tafipolsky M, Schmid R, Johannsmann D, Woll C. Physical chemistry chemical physics : PCCP. 2010; 12:8092–8097. [PubMed: 20532258]

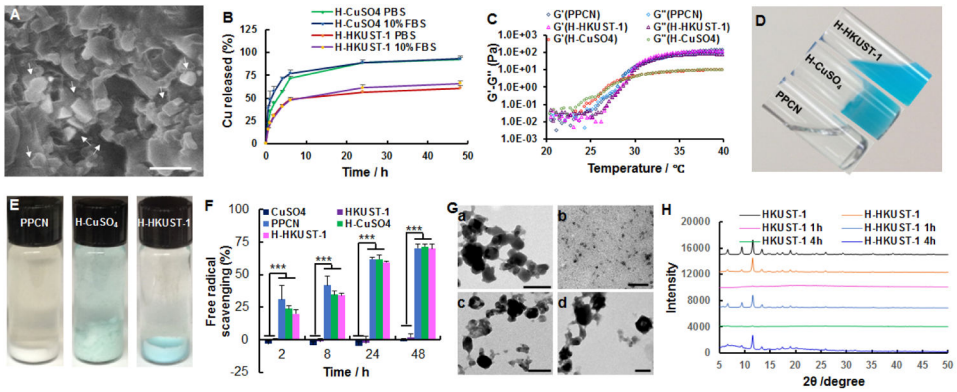

Figure 1.

Characterization of H-HKUST-1. A) SEM digital image of H-HKUST-1. White arrows point to HKUST-1 NPs. (Scale bar: 500 nm). B) Copper release from H-HKUST-1 and H-$CuSO_4$ in PBS or 10% FBS. C) Rheological characterization of PPCN, H-HKUST-1 and H-$CuSO_4$. The storage modulus G′ and loss modulus G″ were plotted logarithmically against temperature (20 – 40°C at 10 Hz) for the corresponding hydrogel samples. D) Digital images of PPCN, H-$CuSO_4$, and H-HKUST-1 at 22°C. E) Digital images of PPCN, H-$CuSO_4$, and H-HKUST-1 after incubation in 10% FBS at 37°C. F) ABTS radical scavenging capacity of $CuSO_4$, HKUST-1 NPs, PPCN, H-$CuSO_4$ and H-HKUST-1. (n = 3, ***P<0.001). G) TEM showing the morphology of (a, b) HKUST-1 NPs and (c, d) H-HKUST-1 before (a, c) and after (b, d) incubation in 10% FBS at 37°C. (Scale bars: 200 nm). H) XRD patterns of HKUST-1 NPs and H-HKUST-1 before and after incubation in 10% FBS.

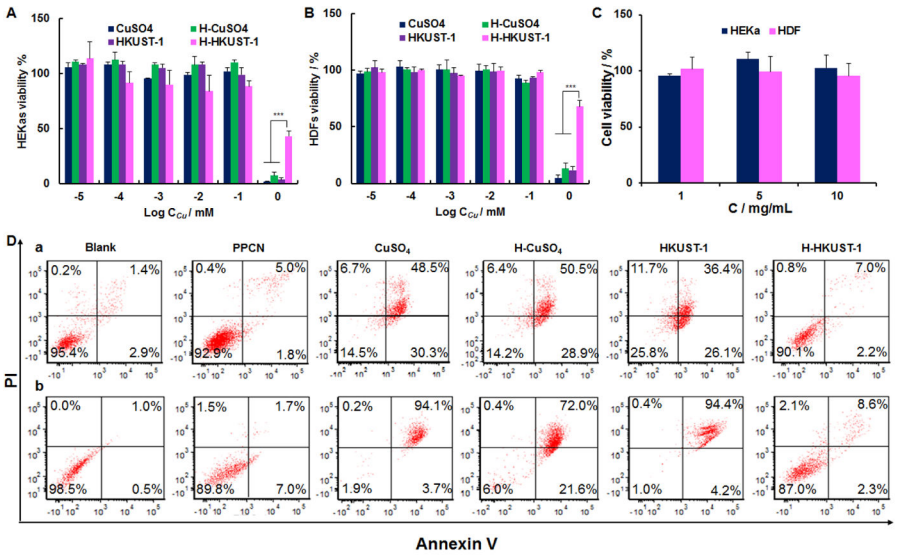

Figure 2.

Cytotoxicity and pro-apoptosis evaluation. Cytotoxicity of $CuSO_4$, H-$CuSO_4$, HKUST-1 NPs and H-HKUST-1 to (A) HEKa and (B) HDF cells. (n = 3, ***$P < 0.001$). C) Cytotoxicity of PPCN to HEKa and HDF cells. D) Cell apoptosis of (a) HEKa cells and (b) HDF cells after treatment with PPCN, $CuSO_4$, H-$CuSO_4$, HKUST-1 NPs or H-HKUST-1 with a copper concentration of 0.5 mM where applicable.

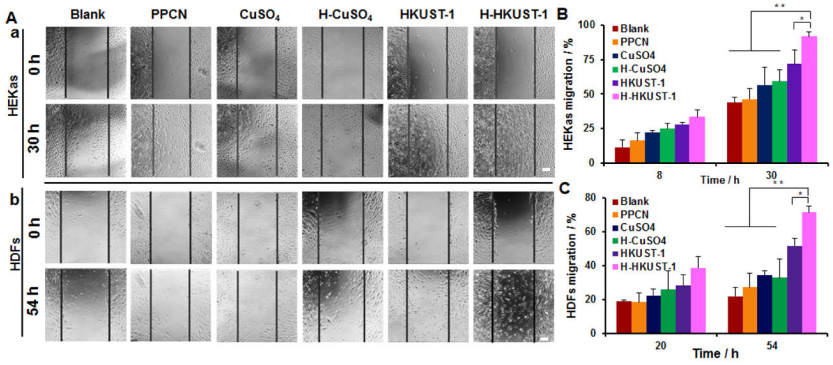

Figure 3.

Effects of H-HKUST-1 on cell migration. A) Digital images of (a) HEKa cells and (b) HDF cells after treatment with PPCN, $CuSO_4$, H-$CuSO_4$, HKUST-1 NPs, or H-HKUST-1 for 0 hr and 30 hrs or 54 hrs at a copper concentration of 1 μM. Quantitative analysis of (B) HEKa cell and (C) HDF cell migration after treatment with PPCN, $CuSO_4$, H-$CuSO_4$, HKUST-1 NPs, and H-HKUST-1. (Scale bar: 50 μm; n = 3, *$p < 0.05$, **$P < 0.01$).

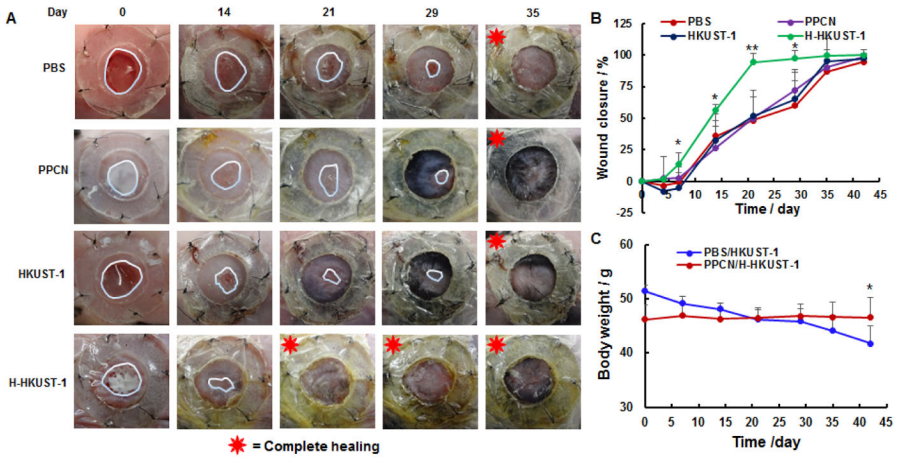

Figure 4.

Effects of H-HKUST-1 on chronic wound healing *in vivo*. A) Digital images of wounds treated with PBS, PPCN, HKUST-1 NPs, or H-HKUST-1. B) Quantitative analysis of wound closure rates. C) Mice body weight changes after PBS, PPCN, HKUST-1 NPs or H-HKUST-1 treatment. (n = 6, $*p < 0.05$, $**P < 0.01$).

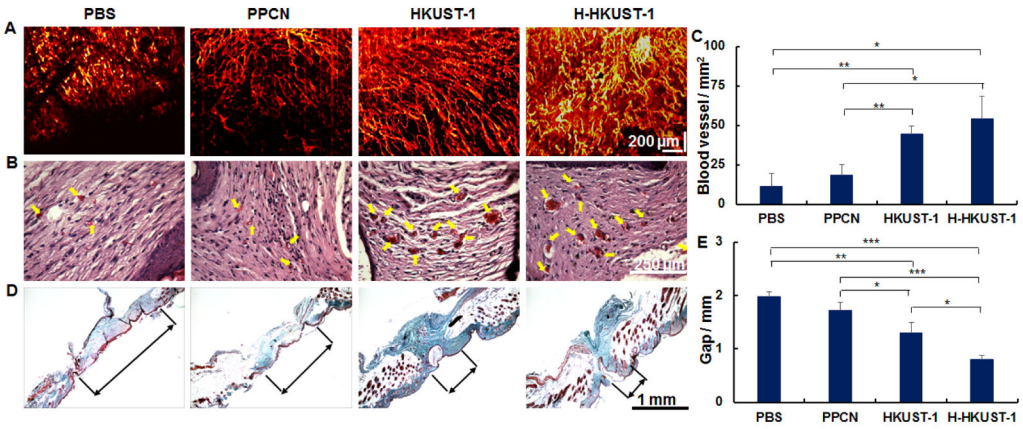

Figure 5.

Analysis of healed wounds. A) Blood vessels observed by OCTA on day 32. B) Blood vessels (arrows) observed after H&E staining. C) Quantification of blood vessel density in H&E-stained tissue sections. D) Collagen distribution (light green) in healed skin as per Masson's trichrome stained tissue sections. E) Quantification of granulation tissue gap measured in Masson's trichrome stained tissue sections. (n=6, $*p < 0.05$, $**P < 0.01$, $***P < 0.001$).